

Structures and Isomeric Transitions of  $\text{NH}_4^+(\text{H}_2\text{O})_{3-6}$ : From Single to Double RingsYih-Sheng Wang,<sup>†</sup> Hai-Chou Chang,<sup>‡</sup> Jyh-Chiang Jiang,<sup>‡</sup> Sheng H. Lin,<sup>†,‡</sup>  
Yuan T. Lee,<sup>†,‡</sup> and Huan-Cheng Chang<sup>\*,‡</sup>*Contribution from the Department of Chemistry, National Taiwan University, Taipei, Taiwan 106, R.O.C., and Institute of Atomic and Molecular Sciences, Academia Sinica, P.O. Box 23-166, Taipei, Taiwan 106, R.O.C.*

Received January 26, 1998

**Abstract:** The  $\text{NH}_4^+(\text{H}_2\text{O})_{3-6}$  cluster ions synthesized by a free jet expansion contain a variety of structural isomers. This investigation identifies some of these isomers by employing vibrational predissociation spectroscopy (VPS) in conjunction with ab initio calculations. The  $\text{NH}_4^+(\text{H}_2\text{O})_n$  ions are produced by corona discharge of  $\text{NH}_3/\text{H}_2\text{O}$  seeded in a  $\text{H}_2$  beam. They are mass-selected and then vibrationally cooled in an octopole ion trap for infrared spectroscopic measurements. In the VPS, four distinct stretching vibrations (hydrogen-bonded and non-hydrogen-bonded NH and OH) are closely examined. The characteristic absorptions of these stretches, together with systematic temperature dependence measurements of their band intensities, allow us to identify both cyclic and noncyclic isomers in the supersonic jet. Such identification is corroborated by ab initio calculations performed at the B3LYP and MP2 levels using the 6-31+G\* basis set. The satisfactory agreement in both vibrational frequencies and absorption intensities between observations and calculations demonstrates that small-sized  $\text{NH}_4^+(\text{H}_2\text{O})_n$  cluster ions can be structurally determined in the gas phase.

## Introduction

Identifying isomeric structures of atomic and molecular clusters is a subject of current interest,<sup>1</sup> with interest rapidly expanding owing to the development of modern spectroscopic techniques for characterizing these species. Related research is also facilitated by advances in ab initio calculations and molecular dynamics simulations, which can now accurately predict the structures and properties of large complex systems. The neutral clusters  $\text{Ar}_n\text{HF}$  and  $(\text{H}_2\text{O})_n$  serve as two citable examples;<sup>2,3</sup> the molecular structures and potential-energy surfaces of them have been determined, both experimentally and theoretically, for species containing more than two individual entities. The structures commonly found for homogeneous molecular trimers, such as  $(\text{HCN})_3$  and  $(\text{H}_2\text{O})_3$ ,<sup>4,5</sup> in a supersonic jet are either linear or cyclic. Recent emphases in this area have shifted toward a search for three-dimensional geometrical configurations as the fascinating architects of fullerenes.<sup>6</sup> Remarkably, a previous study proposed a cagelike structure held together by eight hydrogen bonds upon matching the observed far-infrared spectrum with that predicted by Monte Carlo simulations for  $(\text{H}_2\text{O})_6$ .<sup>7</sup> The latest infrared spectroscopy

of  $(\text{H}_2\text{O})_8$  and  $(\text{H}_2\text{O})_8$ -benzene clusters<sup>8</sup> further indicated that ice cubes with two isomeric forms,  $D_{2d}$  and  $S_4$ , can be synthesized by a free jet expansion. Ab initio calculations confirmed the identification of these isomers.

Previous pulsed electron high-pressure mass spectrometry,<sup>9</sup> which measures the heat of formation and hydration enthalpy of ionic species, revealed the presence of isomeric cluster ions in the gas phase. The measurement aptly illustrated the geometric isomerism of  $\text{C}_2\text{H}_7^+$ , in particular.<sup>10</sup> The protonated ethane can exist either in a classical form,  $\text{C}_2\text{H}_5^+-\text{H}_2$ , or nonclassically as  $\text{H}_3\text{C}(\text{H}^+)\text{CH}_3$  with the proton bridging the two carbon atoms, forming a triangular ring. Infrared spectroscopic experiments by Yeh et al.<sup>11</sup> demonstrated the isomerism by recording a dramatically temperature-dependent CH stretching spectrum of this species in a supersonic beam. The temperature dependence measurement is an effective means of finding isomers of other cluster ions as well. Thermal isomerization studies on isolated  $(\text{CsX})_m\text{Cs}_n^-$  ( $\text{X} = \text{Cl}, \text{Br}, \text{I}$ ) clusters indicated that slight changes in source nozzle temperature upon adiabatic expansion can produce dramatic changes in the distribution of cluster isomers.<sup>12</sup> Such changes suggest an active means of controlling isomer synthesis. This control, in addition to its practical nature, is fundamentally important, since knowing the

<sup>†</sup> National Taiwan University.<sup>‡</sup> Institute of Atomic and Molecular Sciences.(1) See, for example, the special issue of *Science (Washington, D.C.)* **1996**, 271.(2) Liu, S.; Bacic, Z.; Moskowitz, J. W.; Schmidt, K. E. *J. Chem. Phys.* **1995**, 103, 1829 and references therein.(3) Estrin, D. A.; Paglieri, L.; Corongiu, G.; Clementi, E. *J. Phys. Chem.* **1996**, 100, 8701 and references therein.(4) Jucks, K. W.; Miller, R. E. *J. Chem. Phys.* **1988**, 88, 2196.(5) Liu, K.; Loeser, J. G.; Elrod, M. J.; Host, B. C.; Rzepiela, J. A.; Pugliano, N.; Saykally, R. J. *J. Am. Chem. Soc.* **1994**, 116, 3507. Viant, M. R.; Cruzan, J. D.; Lucas, D. D.; Brown, M. G.; Liu, K.; Saykally, R. J. *J. Phys. Chem. A* **1997**, 101, 9032.(6) See, for example, Kroto, H. W., Fischer, J. E., Cox, D. E., Eds.; *The Fullerenes*; Pergamon: Oxford, 1993.(7) Liu, K.; Brown, M. G.; Carter, C.; Saykally, R. J.; Gregory, J. K.; Clary, D. C. *Nature* **1996**, 381, 501. Liu, K.; Brown, M. G.; Saykally, R. J. *J. Phys. Chem. A* **1997**, 101, 8995.(8) Gruenloh, C. J.; Carney, J. R.; Arrington, C. A.; Zwier, T. S.; Fredericks, S. Y.; Jordan, K. D. *Science (Washington, D.C.)* **1997**, 276, 1678. Buck, U.; Ettischer, I.; Melzer, M.; Buch, V.; Sadlej, J. *Phys. Rev. Lett.* **1998**, 80, 2578.(9) Kebarle, P. *Annu. Rev. Phys. Chem.* **1977**, 28, 455.(10) Hiraoka, K.; Kebarle, P. *J. Am. Chem. Soc.* **1976**, 98, 6119.(11) Yeh, L. I.; Price, J. M.; Lee, Y. T. *J. Am. Chem. Soc.* **1989**, 111, 5597.(12) Fatemi, F. K.; Fatemi, D. J.; Bloomfield, L. A. *Phys. Rev. Lett.* **1996**, 77, 4895.

**Table 1.** Experimentally Determined Hydration Energies of the Clustering  $\text{NH}_4^+\text{S}_{n-1} + \text{S} \rightarrow \text{NH}_4^+\text{S}_n$ , Where  $\text{S} = \text{NH}_3$  and  $\text{H}_2\text{O}$ 

$n-1,$ $n$	$\Delta H_{n-1,n}^\circ$ (kcal/mol)				
	S = H <sub>2</sub> O		S = NH <sub>3</sub>		
	PCK <sup>a</sup>	M <sup>b</sup>	SK <sup>c</sup>	PCK <sup>a</sup>	AF <sup>d</sup>
0, 1	-17.3	-19.9	-27	-24.8	-21.5
1, 2	-14.7	-12.4	-17	-17.5	-16.2
2, 3	-13.4	-12.2	-16.5	-13.8	-13.5
3, 4	-12.2	-10.8	-14.5	-12.5	-11.7
4, 5	-9.7	-10.6	-7.5	-9.5	-7.0
5, 6		-9.1			-6.5
6, 7		-8.4			

<sup>a</sup> Payzant, J. D.; Cunningham, A. J.; Kebarle, P. *Can. J. Chem.* **1973**, *51*, 3252. <sup>b</sup> Reference 21. <sup>c</sup> Searles, S. K.; Kebarle, P. *J. Phys. Chem.* **1968**, *72*, 742. <sup>d</sup> Arshadi, M. R.; Futrell, J. H. *J. Phys. Chem.* **1974**, *78*, 1482.

structures of the species studied is a prerequisite for thoroughly understanding their spectroscopic and dynamic behaviors. How isomeric structures influence dissociation dynamics has been investigated by Castleman and co-workers<sup>13</sup> who provided indirect experimental evidence for the existence of two isomers for  $\text{NH}_3((\text{C}_2\text{H}_5)_3\text{N})_3\text{H}^+$  based upon time-of-flight mass spectrometry.

Earlier infrared spectroscopic studies<sup>14</sup> of molecular cluster ions primarily focus on how vibrational frequencies vary with cluster sizes, from which structural information is obtained. Thorough exploration in this direction has been made on  $\text{NH}_4^+(\text{NH}_3)_n$  using vibrational predissociation spectroscopy (VPS) in a supersonic jet.<sup>15,16</sup> For  $\text{NH}_4^+(\text{NH}_3)_{1-8}$ , the clusters are observed to display little structural isomerism. Such an observation is understandable, since the bonding between the solvent molecules is substantially weaker than that between  $\text{NH}_3$  and the  $\text{NH}_4^+$  ion core (Table 1). Additionally,  $\text{NH}_3$  has only one free electron lone pair, averting the complexity that might arise due to multiple hydrogen bond formation on the N end. Because they lack these unique characteristics, the spectroscopy of water-containing clusters, such as  $\text{H}_3\text{O}^+(\text{H}_2\text{O})_n$  and  $\text{NH}_4^+(\text{NH}_3)_m(\text{H}_2\text{O})_n$ ,<sup>17-20</sup> is considerably complicated by the presence of structural isomers as  $n$  increases. Assigning the spectral features is a somewhat more difficult task, disallowing unambiguous identification of the isomeric structures of these clusters. Crofton et al.<sup>20</sup> offered preliminary results of the mixed cluster ions of  $m+n=4$  and proposed three possible isomers for  $\text{NH}_4^+(\text{NH}_3)_3(\text{H}_2\text{O})$ . However, to our knowledge, no ab initio calculations have been performed to verify their propositions.

In this study, we investigate the structural isomerism of  $\text{NH}_4^+(\text{H}_2\text{O})_n$ . A number of measurements<sup>9,21</sup> and calculations<sup>22-26</sup>

(13) Wei, S.; Tzeng, W. B.; Castleman, A. W., Jr. *J. Phys. Chem.* **1990**, *94*, 6927.

(14) See a recent review, Bieske, E. J.; Maier, J. P. *Chem. Rev.* **1993**, *93*, 2603.

(15) Price, J. M.; Crofton, M. W.; Lee, Y. T. *J. Chem. Phys.* **1989**, *91*, 2749; *J. Phys. Chem.* **1991**, *95*, 2182.

(16) Ichihashi, M.; Yamabe, J.; Murai, K.; Nonose, S.; Hirao, K.; Kondow, T. *J. Phys. Chem.* **1996**, *100*, 10050.

(17) Yeh, L. I.-C.; Okumura, M.; Myers, J. D.; Price, J. M.; Lee, Y. T. *J. Chem. Phys.* **1989**, *91*, 7319.

(18) Price, J. M. Ph.D. Thesis, University of California, Berkeley, 1990; Chapter II.

(19) Price, J. M. Ph.D. Thesis, University of California, Berkeley, 1990; Chapter IV.

(20) Crofton, M. W.; Price, J. M.; Lee, Y. T. In *Clusters of Atoms and Molecules*; Haberland, H., Ed.; Springer-Verlag: Berlin, 1994; p 45.

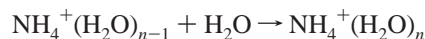
(21) Meot-Ner, M. *J. Am. Chem. Soc.* **1984**, *106*, 1265.

(22) Pullman, A.; Claverie, P.; Cluzan, M.-C. *Chem. Phys. Lett.* **1985**, *117*, 419.

(23) Kassab, E.; Evleth, E. M.; Hamou-Tahra, Z. D. *J. Am. Chem. Soc.* **1990**, *112*, 103.

(24) Armstrong, D. A.; Rauk, A.; Yu, D. *Can. J. Chem.* **1993**, *71*, 1368.

have been made for this fundamental system concerning the clustering with the hydration energy  $\Delta H_{n-1,n}^\circ$ ,



Calculations<sup>23</sup> for the cluster  $\text{NH}_4^+(\text{H}_2\text{O})_4$  in its most stable configuration revealed that the first solvation shell contains four  $\text{H}_2\text{O}$  molecules, symmetrically forming four hydrogen bonds around the ion. Pulsed electron high-pressure mass spectrometric measurements<sup>21</sup> indicated that the energy deemed necessary to form the first hydrogen bond between  $\text{NH}_4^+$  and  $\text{H}_2\text{O}$  is  $\Delta H_{0,1}^\circ = -19$  kcal/mol. The  $-\Delta H_{n-1,n}^\circ$  monotonically decreases with  $n$  to  $\sim 10$  kcal/mol at  $n > 4$ , a behavior analogous to  $\text{H}_3\text{O}^+(\text{H}_2\text{O})_n$  and many other ionic systems.<sup>21</sup> As noted from Table 1, the bonding of  $\text{NH}_4^+$  with  $\text{H}_2\text{O}$  is considerably weaker than that with  $\text{NH}_3$  by 2–7 kcal/mol, depending on the measurements. Unlike that in  $\text{NH}_4^+(\text{NH}_3)_n$ , there is no clear discontinuity in  $\Delta H_{n-1,n}^\circ$  for  $\text{NH}_4^+(\text{H}_2\text{O})_n$  between  $\Delta H_{3,4}^\circ$  and  $\Delta H_{4,5}^\circ$  when the first hydration shell begins to fill. The finding suggests that structural isomerization can occur at  $n$  as small as 4 in the ammonium–water cluster ions.

As a result of its molecular simplicity, the system  $[\text{NH}_3(\text{H}_2\text{O})_n]\text{H}^+$  has been considered<sup>27</sup> as a prototype for exploring hydrogen bonding and proton-transfer dynamics of protonated ions in water. Molecular dynamics simulations<sup>28,29</sup> also closely examined the rotational motions of ammonium ions in water, as it is a model system for studying proton exchange between  $\text{H}_2\text{O}$  and protonated amines.<sup>30</sup> Spectroscopically, the  $\text{NH}_4^+(\text{H}_2\text{O})_n$  cluster benefits from its unique nature in that it has both NH and OH stretching vibrations to be explored. Since these two stretches are distinct in frequencies, in combination with the characteristic band shifting of hydrogen- and non-hydrogen-bonded stretches, at least four possible spectral signatures can be identified. Such identification lays a solid foundation for unambiguously assigning the spectral features to each structural isomer. The assignment is essential for structurally determining the isomers, since in these clusters, the number of isomers increases exponentially with  $n$ , and furthermore, the difference in energy between isomers gradually diminishes at a larger  $n$ .<sup>31</sup> In this work we demonstrate that, based upon the spectroscopic measurements and the latest ab initio calculations,<sup>32</sup> a number of structural isomers can be unambiguously identified for  $\text{NH}_4^+(\text{H}_2\text{O})_{3-6}$  synthesized in a corona-discharged molecular beam.

## Experimental Section

Figure 1 schematically depicts the vibrational predissociation ion-trap (VPIT) spectrometer. Briefly, the VPIT spectrometer consists of five major units: (1) a corona discharge ion source, (2) a sector magnet mass spectrometer, (3) a radio frequency octopole ion trap, (4) a quadrupole mass filter, and (5) a Daly detector. Between these units, a number of electrostatic lenses and optics were used to focus, shape, bend, accelerate, and decelerate the ion beam. Details of the apparatus have been previously described.<sup>15,17,33</sup>

(25) Bueker, H.-H.; Uggerud, E. *J. Phys. Chem.* **1995**, *99*, 5945.

(26) Contador, J. C.; Aguilar, M. A.; Olivares del Valle, F. *J. Chem. Phys.* **1997**, *214*, 113.

(27) Cheng, H.-P. *J. Chem. Phys.* **1996**, *105*, 6844.

(28) Jorgensen, W. L.; Gao, J. *J. Phys. Chem.* **1986**, *90*, 2174.

(29) Karim, O. A.; Haymet, A. D. *J. Chem. Phys.* **1990**, *93*, 5961.

(30) Perrin, C. L.; Gipe, R. K. *Science (Washington, D.C.)* **1987**, *238*, 1393.

(31) Berry, R. S. *Chem. Rev.* **1993**, *93*, 2379 and references therein.

(32) Jiang, J. C.; Chang, H.-C.; Lee, Y. T.; Lin, S. H. Manuscript in preparation.

(33) Bustamente, S. W.; Okumura, M.; Gerlich, D.; Kwok, H. S.; Carlson, L. R.; Lee, Y. T. *J. Chem. Phys.* **1987**, *86*, 508.

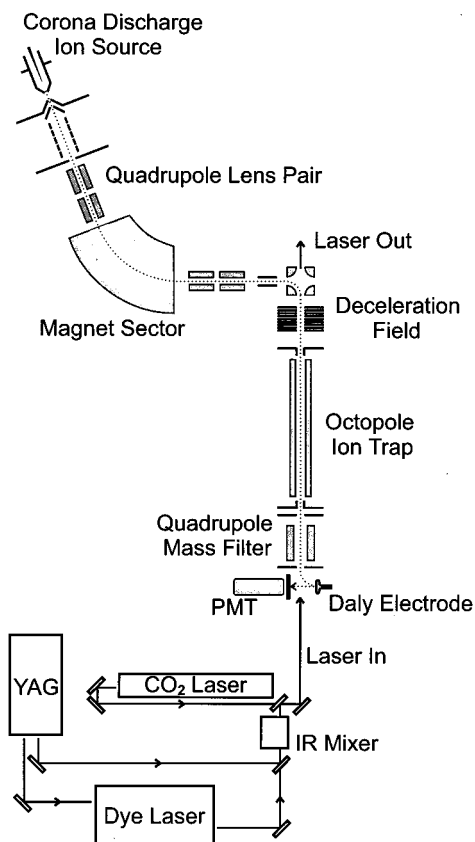


**Figure 1.** Experimental layout and the vibrational predissociation ion-trap spectrometer. Detailed descriptions of the apparatus can be found in refs 15 and 17.

Herein, we synthesized the ammonium ions by corona discharge of  $\text{NH}_3/\text{H}_2\text{O}$  vapor seeded in pure  $\text{H}_2$  at a backing pressure of roughly 100 Torr. The ions were then supersonically expanded through a  $75 \mu\text{m}$  nozzle, allowing complexation of  $\text{NH}_4^+$  with  $\text{H}_2\text{O}$  to be established. Since the proton affinity of  $\text{NH}_3$  exceeds that of  $\text{H}_2\text{O}$  by 37.5 kcal/mol,<sup>34</sup>  $\text{NH}_4^+$  was preferentially formed. While some of the  $\text{H}_2\text{O}$  molecules can also be protonated, owing to energetic favorability of  $\text{NH}_4^+$  formation, proton transfer immediately occurs via binary collisions when  $\text{H}_3\text{O}^+$  encounters  $\text{NH}_3$ . The rotational temperature of the clusters is expected to be  $\sim 50 \text{ K}$ .<sup>15</sup> The ion beam, after passing through the skimmer, was focused by a pair of quadrupole lenses into a sector magnet mass spectrometer, which selected the protonated cluster ions [ $\text{NH}_4^+(\text{H}_2\text{O})_n$ ] of interest. The emitted beam was then guided by a  $90^\circ$  quadrupole bending field toward an octopole ion trap. Following deceleration to a kinetic energy of  $\sim 1 \text{ eV}$ , the selected ions were stored in the ion trap for about 1 ms before infrared laser irradiation. The storage not only increased the concentration of the ions interrogated but also reduced the number of metastable ions, which are unwanted background in detection. A quadrupole mass filter, equipped with a Daly detector operating in an ion-counting mode, monitored the concentration increase of the dissociating daughter ions [ $\text{NH}_4^+(\text{H}_2\text{O})_{n-1}$ ] upon laser irradiation to obtain a background-minimized spectrum. The vibrationally induced dissociation typically finishes in less than  $20 \mu\text{s}$ , as determined by direct time-domain measurements.

The laser systems used in this experiment consisted of an yttrium aluminum garnet (YAG) laser (Infinity, Coherent), a dye laser (Scanmate, Lambda-Physics), and a difference frequency mixer (Autotracker, Inrad). The pulsed infrared laser was generated by difference frequency mixing of the dye laser with the YAG fundamental photons and was employed both as the excitation and as the fragmentation light source. The laser, operated at 20 Hz with about 1–4 mJ in a 3.5-ns pulse, resonantly excited the ion–molecule complexes at  $2600\text{--}4000 \text{ cm}^{-1}$  from  $v = 0$  to  $v = 1$ . In this experiment, the typical number of ions

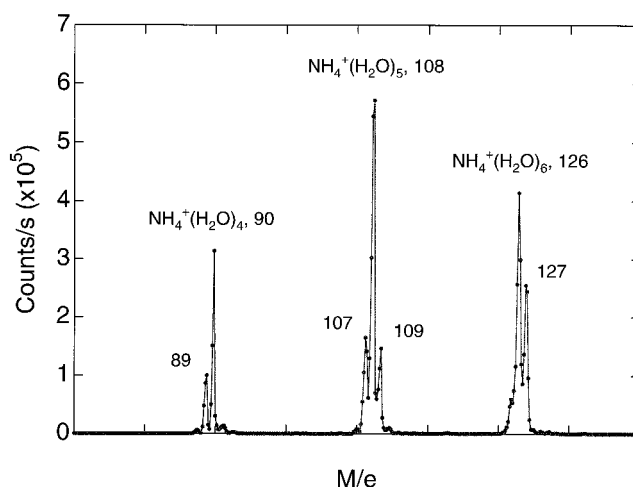


**Figure 2.** Typical mass spectrum obtained by the sector magnet mass spectrometer for  $\text{NH}_4^+(\text{H}_2\text{O})_n$ . The spectrum was taken when the beam conditions were optimized at  $n = 5$  of  $M/e = 108$ . The features adjacent to the  $\text{NH}_4^+(\text{H}_2\text{O})_{4-6}$  peaks are those of the mixed cluster ions  $\text{NH}_4^+(\text{NH}_3)_m(\text{H}_2\text{O})_n$  and  $\text{H}_3\text{O}^+(\text{H}_2\text{O})_n$ , which have  $M/e$  ratios differing by one unit. The closely spaced components, however, can be adequately separated by the mass spectrometer with a typical mass resolution of  $M/\Delta M > 200$ .

stored in the trap was  $\sim 400$  ions/pulse. The spectra shown in the following figures were normally obtained by averaging 200 shots of the ion pulses. As a result of the weakness of the laser power and also the smallness of the vibrational absorption cross section, only about 1% of the total ions was depleted. This level of depletion, nevertheless, gives sufficient S/N ratios for observation, since the inherent electronics noises contribute less than 0.2 counts/pulse. The observed noises in the power-normalized spectra are thus derived predominantly from the metastable background ions, laser power fluctuation, and atmospheric water absorptions at  $\sim 2.9 \mu\text{m}$ . As the corona-discharged ion beam is relatively hot, the number of metastable ions (typically 1% of the total) increases with  $n$  due to weaker hydrogen bonding involved in larger clusters (Table 1). The undesired background ions subsequently become the dominant source of noises in those cases. The spectral line width of the present infrared laser is  $\sim 0.2 \text{ cm}^{-1}$ , and the uncertainty in absolute frequency measurements is  $\pm 1 \text{ cm}^{-1}$ .

Figure 2 displays a typical mass spectrum of the ammonium-ion–water clusters synthesized by the corona-discharged jet expansion. The spectrum was taken after optimization for the cluster ion  $\text{NH}_4^+(\text{H}_2\text{O})_5$  at  $M/e = 108$ . As a result of the lack of selectivity in ion formation, other unwanted species, for example, the mixed  $\text{NH}_4^+(\text{NH}_3)_m(\text{H}_2\text{O})_n$  ions, were also produced in the beam. The relative abundance of these ions heavily relies on the gas compositions,  $[\text{NH}_3]/[\text{H}_2\text{O}]/[\text{H}_2]$  and on the beam expansion conditions. In Figure 2, the cluster ions in each mass manifold ( $m + n = 4, 5$ , or  $6$ ) differ by only one  $M/e$  unit, and they must be sufficiently separated to avert cross contamination. This stringent requirement reflects the major effort in the present experiment: optimizing the conditions to generate the maximal number of ions and, simultaneously, establishing a sufficient mass resolution of  $M/\Delta M > 200$  for ion separation. To actively control the isomer synthesis, the beam temperature was varied by adjusting the source nozzle temperature from 360 to 240 K and the nozzle backing pressure from 50 to 250 Torr.

**Ab Initio Calculations.** The ab initio calculations for the  $\text{NH}_4^+(\text{H}_2\text{O})_n$  cluster ions were performed using the program package GAUSSIAN 94 on two different levels (B3LYP/6-31+G\* and MP2/6-31+G\*). Details of the calculations can be found elsewhere.<sup>32</sup> For simplicity, most of the results presented herein involve only the calculations employing Becke3LYP functional with the 6-31+G\* basis set on both the  $\text{NH}_4^+$  ion core and the solvent water molecules. The geometries were optimized using analytical gradients, and the harmonic vibrational frequencies were obtained using analytical second derivatives. Also determined herein were the binding energies and the infrared absorption intensities of various structural isomers to be compared with

(34) Lias, S. G.; Liebman, J. F.; Levin, R. D. J. *Phys. Chem. Ref. Data* 1984, 13, 695.

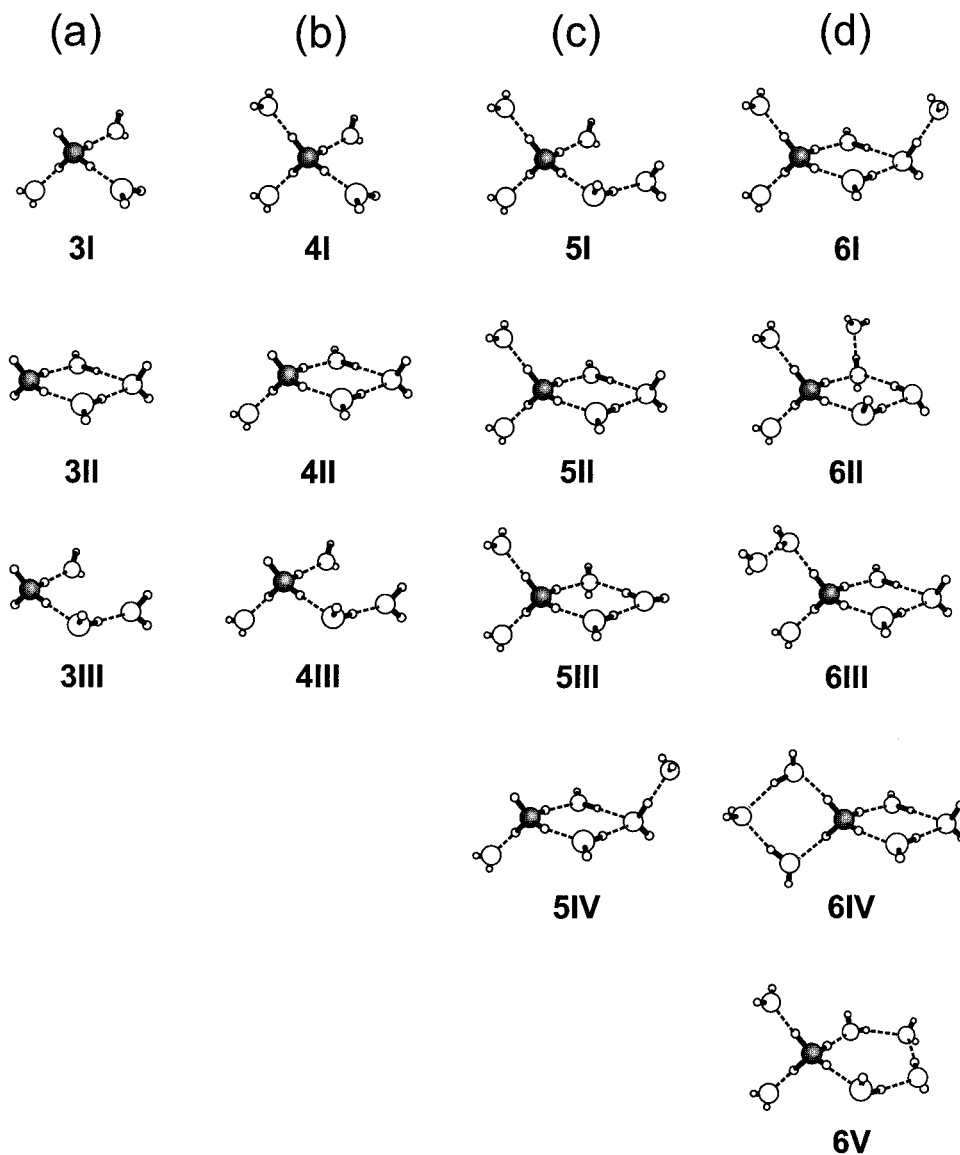


**Figure 3.** Optimized geometries given by the ab initio calculations for  $\text{NH}_4^+(\text{H}_2\text{O})_{3-6}$ . The N, O, and H atoms are denoted by ●, ○, and ○, respectively.

measurements. The scaling factor for the calculated frequencies is 0.973, which was chosen by referring to the experimentally observed free-OH stretching frequencies of two- and three-coordinated  $\text{H}_2\text{O}$  in  $\text{NH}_4^+(\text{H}_2\text{O})_6$ .<sup>35</sup>

Figure 3 illustrates the optimized geometrical configurations predicted by the ab initio calculations for  $\text{NH}_4^+(\text{H}_2\text{O})_{3-6}$ . In addition to these structures, other low-energy isomers are found in the calculations as well. For  $\text{NH}_4^+(\text{H}_2\text{O})_{3-5}$ , species **3I–3III**, **4I–4III**, **5I**, **5II**, and **5IV** represent, separately, the three lowest-energy structures in each solvation group. Compared to other isomers, they are lower in energy by more than 1 kcal/mol.<sup>32</sup> For  $\text{NH}_4^+(\text{H}_2\text{O})_6$ , an extensive search for isomers was not attempted, and therefore the structures **6I–6V** represent the isomers that are most likely to be observed in this experiment where water molecules are sequentially attached to the ion core during the supersonic expansion. Table 2 lists the calculated energetics of isomeric  $\text{NH}_4^+(\text{H}_2\text{O})_{3-6}$  using the 6-31+G\* basis set at both the B3LYP and the MP2 levels. As noted, these values depend significantly on the form of the isomers, although they all successfully reproduce the measurements (Table 1). Since the structures of the clusters remain unknown in the hydration energy measurements, the experimentally determined numbers listed in Table 1 should be considered as average values.

(35) Wang, Y.-S.; Jiang, J. C.; Cheng, C.-L.; Lin, S. H.; Lee, Y. T.; Chang, H.-C. *J. Chem. Phys.* **1997**, *107*, 9695.

As will be demonstrated in a separate publication,<sup>32</sup> the B3LYP/6-31+G\* calculation is fairly good in describing the hydrogen-bond interactions between protonated ions and water molecules. Compared to MP2/6-31+G\*, it offers the advantage of being less computationally demanding. From detailed studies of  $\text{NH}_4^+(\text{H}_2\text{O})_{1-5}$ ,<sup>32</sup> we concluded that MP2/6-31+G\* is better in predicting the interaction energy between  $\text{NH}_4^+$  and  $\text{H}_2\text{O}$ , whereas B3LYP/6-31+G\* tends to overestimate it (Table 2). As for vibrational frequencies, the two methods provide similar values, with a typical difference of less than 0.5% for free-OH and 3% for bonded-OH stretches, although the MP2/6-31+G\* computation requires much more disk space in handling larger clusters. An elaborate comparison between the density-functional and the MP2 methods has been previously given by Xantheas<sup>36</sup> for cyclic water clusters.

## Results and Analysis

Figure 4 presents an overview diagram of the vibrational predissociation spectra of  $\text{NH}_4^+(\text{H}_2\text{O})_{3-6}$ . It displays the smooth changes in both frequency and intensity of the NH and OH stretches with the solvation number.<sup>37</sup> The spectra of the individual clusters are discussed as follows.

(36) Xantheas, S. S. *J. Chem. Phys.* **1995**, *102*, 4505.

**Table 2.** Ab-Initio-Calculated Hydration Energies (kcal/mol) of the Clustering (1)  $\text{NH}_4^+ + n\text{H}_2\text{O} \rightarrow \text{NH}_4^+(\text{H}_2\text{O})_n$  and (2)  $\text{NH}_4^+(\text{H}_2\text{O})_{n-1} + \text{H}_2\text{O} \rightarrow \text{NH}_4^+(\text{H}_2\text{O})_n$ , using B3LYP/6-31+G\* and MP2/6-31+G\*<sup>a</sup>

isomers		B3LYP/6-31+G*		MP2/6-31+G*	
$\text{NH}_4^+(\text{H}_2\text{O})_{n-1}$	$\text{NH}_4^+(\text{H}_2\text{O})_n$	$\Delta E_n$	$\Delta E_{n,n-1}$	$\Delta E_n$	$\Delta E_{n,n-1}$
2I <sup>b</sup>	3I	-47.77	-13.02	-45.77	-12.65
2I	3II	-45.86	-11.05	-43.49	-10.45
2I	3III	-45.73	-11.10	-43.01	-10.25
3I	4I	-58.65	-10.82	-56.74	-10.76
3I	4II	-57.92	-10.07	-55.51	-9.62
3I	4III	-57.38	-9.69	-54.76	-9.12
4I	5I	-67.34	-8.76	-64.92	-8.29
4I	5II	-68.04	-9.22	-65.78	-9.03
4I	5III	-65.20	-6.53	-62.92	-6.09
4II	5IV	-68.18	-10.51	-64.80	-9.70
5II	6I	-77.60	-9.97		
5III	6II	-74.94	-9.97		
5II	6III	-76.38	-8.46		
5II	6IV	-77.07	-8.91		
5I	6V	-75.77	-8.56		

<sup>a</sup>  $\Delta E_n$  and  $\Delta E_{n,n-1}$  represent, respectively, the calculated hydration energies of the clustering via channels 1 and 2 with basis set superposition errors and zero-point energies corrected. <sup>b</sup> With the structure:

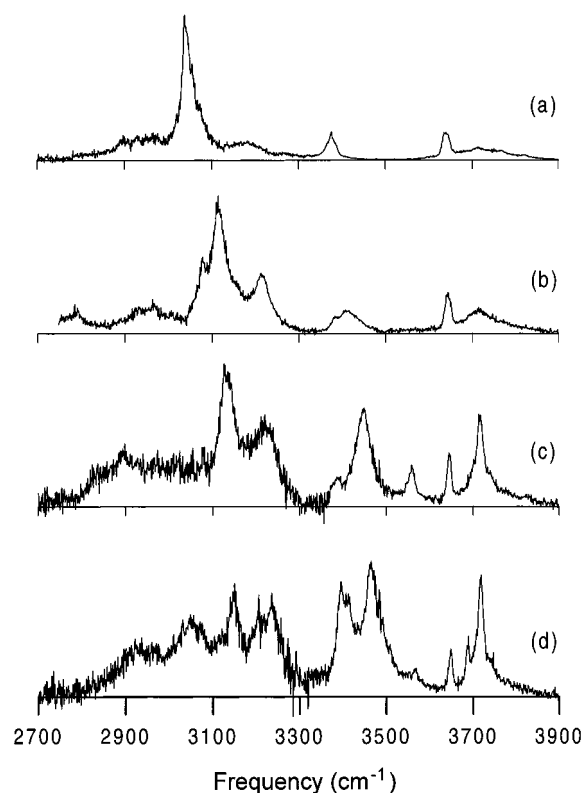
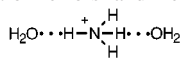


**Figure 4.** Vibrational predissociation spectra of  $\text{NH}_4^+(\text{H}_2\text{O})_n$  at (a)  $n = 3$ , (b)  $n = 4$ , (c)  $n = 5$ , and (d)  $n = 6$  in the NH and OH stretching regions.

**A.  $\text{NH}_4^+(\text{H}_2\text{O})_3$ .** Figure 5 compares the spectrum of  $\text{NH}_4^+(\text{H}_2\text{O})_3$  with the ab initio results calculated at the B3LYP/6-31+G\* level. Three groups of transitions were recorded: hydrogen-bonded-NH stretches at 2900–3200  $\text{cm}^{-1}$ , free-NH stretches at 3300–3450  $\text{cm}^{-1}$ , and free-OH stretches at 3600–3900  $\text{cm}^{-1}$ . These two types of NH stretching are distinguished by referring to the well documented spectrum<sup>38</sup> of free  $\text{NH}_4^+$ ,

(37) Chang, H.-C.; Wang, Y.-S.; Lee, Y. T.; Chang, H.-C. *Int. J. Mass Spectrom. Ion Processes*, in press.

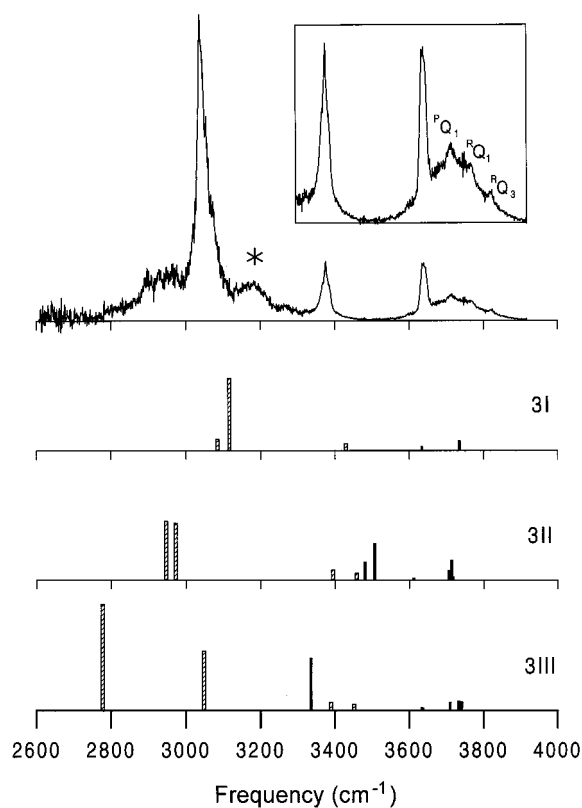


**Figure 5.** Vibrational spectrum of  $\text{NH}_4^+(\text{H}_2\text{O})_3$  in both NH and OH stretching regions. The beam was expanded at a nozzle temperature of 300 K and a backing pressure of 50 Torr. Shown underneath are the ab initio calculated stick diagrams of NH ( $\square$ ) and OH ( $\blacksquare$ ) stretches for the isomers with structures illustrated in Figure 3a. Inset: an enlarged view of the free-OH stretching absorptions where the  $K$ -rotational subbands of  $\text{H}_2\text{O}$  along its local  $C_2$  axis are indicated. The asterisk denotes  $\text{H}_2\text{O}$  bending overtones or  $\text{NH}_4^+$  combination bands.

which has resonances located at 3270 and 3343  $\text{cm}^{-1}$  for the symmetric ( $\nu_1$ ) and asymmetric ( $\nu_3$ ) stretching, respectively. Upon complexation with  $\text{H}_2\text{O}$ , the  $\text{NH}_4^+$  ion exhibits marked frequency red-shifting in its NH stretches. As observed for a variety of neutral and ionic clusters,<sup>14,39</sup> the frequencies of hydrogen-bonded stretches red-shift to a larger measure than non-hydrogen-bonded ones owing to proton donation. For OH stretches, the observed transitions are close in frequency to those of free  $\text{H}_2\text{O}$  at 3657.0 and 3755.7  $\text{cm}^{-1}$ .<sup>40</sup> Within our detection sensitivity, no indication suggests the presence of hydrogen-bonded-OH stretches at the lower-frequency region for this particular cluster. We assign the sharper transition at 3640  $\text{cm}^{-1}$  to the symmetric OH stretches and attribute the broader and more complex features peaking at 3714  $\text{cm}^{-1}$  to the asymmetric OH stretching vibrations of the neutral water molecules. The  $\text{H}_2\text{O}$  in this cluster acts as a single proton acceptor, denoted as  $\text{H}_2\text{O}(\text{A})$ ,<sup>41</sup> with none of its hydrogen atoms participating in the bonding.

The absence of hydrogen-bonded-OH stretching absorptions in Figure 5 suggests a structure for  $\text{NH}_4^+(\text{H}_2\text{O})_3$ : the three  $\text{H}_2\text{O}$  molecules are situated equivalently on the first ( $1^\circ$ ) solvation

(38) Gudeman, C. S.; Saykally, R. J. *Annu. Rev. Phys. Chem.* **1984**, *35*, 387.

(39) Dopfer, O.; Nizkorodov, S. A.; Meuwly, M.; Bieske, E. J.; Maier, J. P. *Int. J. Mass Spectrom. Ion Processes* **1997**, *167/168*, 637.

(40) Herzberg, G. *Molecular Spectra and Molecular Structure, III. Electronic Spectra and Electronic Structure of Polyatomic Molecules*; Van Nostrand-Reinhold: New York, 1966.

(41) The notations follow that of Zwier, Jordan, and co-workers in ref 8.

shell. This structure is indeed confirmed by the ab initio calculations,<sup>32</sup> which forecast that isomer **3I**, illustrated in Figure 3a, is energetically most favorable among the three species; it is  $\sim 2$  kcal/mol more stable than both **3II** and **3III** (Table 2). For isomer **3I**, the calculations further indicate that the ion and the solvent molecules are connected in a linear  $\text{N}-\text{H}\cdots\text{O}$  configuration (with an angle of  $\angle\text{N}-\text{H}\cdots\text{O} = 179.3^\circ$ ) when forming the hydrogen bond. The local  $C_2$  axis of  $\text{H}_2\text{O}$  is collinear with the hydrogen bond, as the interaction between  $\text{NH}_4^+$  and  $\text{H}_2\text{O}$  is dominated by the electrostatic attraction of the ion charge with the water dipole, rather than with one of the two oxygen electron lone pairs.<sup>25</sup>

This work also explores how the  $\text{NH}_4^+(\text{H}_2\text{O})_3$  spectrum varies with beam temperature. The temperature dependence measurements over a wide range showed minor changes in the spectra, revealing that predominantly only one kind of isomer was synthesized by the free jet expansion. Displayed underneath the experimentally observed spectrum in Figure 5 are the ab-initio-calculated stick diagrams for isomers **3I**–**3III**. The simplicity of this spectrum clearly favors the assignment of the  $3375\text{ cm}^{-1}$  band to the single free-NH stretching of isomer **3I**. The assignment correlates well with the sharpness of the feature, with a full width at half-maximum (fwhm) of less than  $30\text{ cm}^{-1}$ . In the bonded-NH stretching region, however, a considerable deviation arises between observations and calculations. The predicted splitting for the three-coupled bonded-NH stretches of isomer **3I** is  $32\text{ cm}^{-1}$ , which is severely underestimated in comparison with the experimentally observed absorptions at  $2962$  and  $3045\text{ cm}^{-1}$ . Although the prediction is substantially off for the bonded-NH stretches, the overall agreement in Figure 5 is satisfactory. We attributed the sharper and more intense feature at  $3045\text{ cm}^{-1}$  to the asymmetric NH vibrations, which are doubly degenerate, and the broader one at  $2962\text{ cm}^{-1}$  to the symmetric NH stretching of the central ion of isomer **3I** (Table 3).

The fine structures<sup>42</sup> built on top of the asymmetric free-OH stretching absorptions in Figure 5 denote the internal rotation of  $\text{H}_2\text{O}$  bound to the ammonium ion core. As in the case of  $\text{NH}_4^+(\text{NH}_3)_3(\text{H}_2\text{O})$ ,<sup>19,20</sup> these structures can be assigned to the  $K$ -rotational subbands of the perpendicular transitions of  $\text{H}_2\text{O}$  rotating along its local  $C_2$  axis. The internal rotation, however, is not as free as that in  $\text{NH}_4^+(\text{NH}_3)_3(\text{H}_2\text{O})$  where the individual Q-branch lines are sharp (fwhm  $\sim 10\text{ cm}^{-1}$ ) and well-resolved. In  $\text{NH}_4^+(\text{NH}_3)_3(\text{H}_2\text{O})$ , the observed separation of the adjacent Q branches is  $29\text{ cm}^{-1}$ , which is nearly identical to  $2B$  where  $B = 14.5\text{ cm}^{-1}$ , the rotational constant of free water molecules. For  $\text{NH}_4^+(\text{H}_2\text{O})_3$ , the three noticeable rotational features in Figure 5 are roughly spaced by  $55\text{ cm}^{-1}$ , and they can be assigned to the  ${}^P\text{Q}_1$ ,  ${}^R\text{Q}_1$ , and  ${}^R\text{Q}_3$  subbands of the asymmetric OH stretching transitions, respectively. The intensity alternation with substantially weaker  ${}^R\text{Q}_2$  and  ${}^R\text{Q}_4$  subbands of even  $K$  is tentatively attributed to proton nucleus spin statistics.<sup>19,20</sup>

**B.  $\text{NH}_4^+(\text{H}_2\text{O})_4$ .** Figure 6 displays the OH stretching spectrum of  $\text{NH}_4^+(\text{H}_2\text{O})_4$  and its dramatic temperature dependence. Comparing the spectra with that of  $\text{NH}_4^+(\text{H}_2\text{O})_3$  clearly indicates that new features emerge at lower-frequency regions for the bonded-OH stretches at  $n = 4$ . The newly observed transitions can be separated into two groups at the wavenumbers

(42) The congestion in the  $K$ -subbands of the free-OH asymmetric stretching of  $\text{NH}_4^+(\text{H}_2\text{O})_3$  cannot be effectively reduced by lowering the beam temperature to  $130\text{ K}$ , which is the lowest temperature that can be achieved in this experiment. While the spectral congestion can be a combined result of small rotational constants, rapid vibrational predissociation, and a relatively high internal temperature yielded by the corona discharge, it is also likely due to hindered rotation caused by neighboring  $\text{H}_2\text{O}$  dipole–dipole coupling (ref 19).

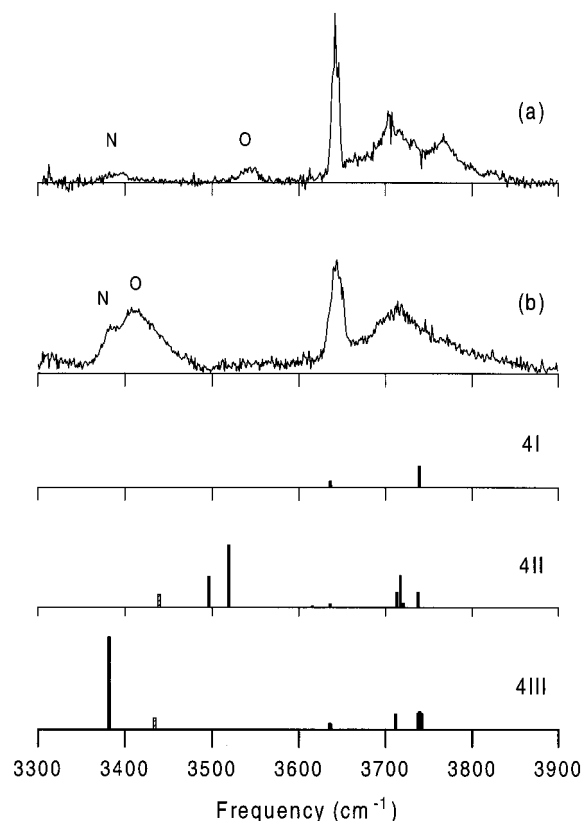


**Figure 6.** Temperature dependence of the vibrational spectra of  $\text{NH}_4^+(\text{H}_2\text{O})_4$  in the OH stretching region. The beam was expanded at a (nozzle temperature, backing pressure) of (a) ( $270\text{ K}$ ,  $130\text{ Torr}$ ) and (b) ( $300\text{ K}$ ,  $60\text{ Torr}$ ). All the spectra are laser-power-normalized. Characters “N” and “O” denote the bands that can be assigned to the free-NH and the bonded-OH stretches, respectively. Shown underneath are the ab-initio-calculated stick diagrams of NH (□) and OH (■) stretches for the isomers with structures illustrated in Figure 3b.

of  $\{3391; 3543\}$  and  $\{3382; 3408\}$ . The latter was observed only when the beam was sufficiently warm. The two transition groups, which have absorption intensities varying independently with beam temperature, evidently originate from two different isomers. The abrupt appearance of the hydrogen-bonded-OH absorptions in Figure 6 suggests that structural isomerization is energetically allowed at this particular cluster size where the fourth  $\text{H}_2\text{O}$  can be attached to either one or two of the three  $1^\circ$   $\text{H}_2\text{O}$  molecules, forming the second shell. The observation of isomers correlates well with the hydration enthalpy measurements mentioned in the Introduction.

The isolated feature at  $3391\text{ cm}^{-1}$  in Figure 6a can be assigned to the free-NH stretching of  $\text{NH}_4^+(\text{H}_2\text{O})_4$ , since its frequency agrees with that of  $\text{NH}_4^+(\text{H}_2\text{O})_3$  to within  $10\text{ cm}^{-1}$ . Compared to Figure 5, the absorption intensity of this free-NH band is much weaker, suggesting that the predominant form of  $\text{NH}_4^+(\text{H}_2\text{O})_4$  synthesized by the present jet expansion has a structure similar to **4I** depicted in Figure 3b. The species contains a filled first solvation shell with no free NH bonds exposed. In identifying the structural isomers, ab initio calculations predict three most probable structures for  $\text{NH}_4^+(\text{H}_2\text{O})_4$ , as illustrated in Figure 3b. Among these three species, isomer **4I** is lowest in energy, consistent with previous predictions.<sup>23</sup> It is  $\sim 1$  kcal/mol more stable than isomer **4II**, a ring-shaped species. In this ring isomer, the perturbed  $1^\circ$   $\text{H}_2\text{O}$  changes its role from a single acceptor to a single-acceptor–single-donor, denoted as  $1^\circ\text{H}_2\text{O}(\text{AD})$ ,<sup>41</sup> upon second shell formation. Comparison of the observed spectrum [Figure 6a] with the ab-initio-calculated diagrams clearly identifies the presence of

**Table 3.** Frequencies ( $\text{cm}^{-1}$ ) and Assignments of the Prominent Features of NH and OH Stretches Observed in the  $\text{NH}_4^+(\text{H}_2\text{O})_{3-6}$  Spectra

species	frequency	isomers <sup>a</sup>	assignments <sup>b</sup>	
$\text{NH}_4^+(\text{H}_2\text{O})_3$	3825	<b>3I</b>	<sup>R</sup> Q <sub>3</sub> , asymmetric free OH of 1° H <sub>2</sub> O(A)	
	3770	<b>3I</b>	<sup>R</sup> Q <sub>1</sub> , asymmetric free OH of 1° H <sub>2</sub> O(A)	
	3714	<b>3I</b>	<sup>P</sup> Q <sub>1</sub> , asymmetric free OH of 1° H <sub>2</sub> O(A)	
	3640	<b>3I</b>	symmetric free OH of 1° H <sub>2</sub> O(A)	
	3375	<b>3I</b>	free NH of $\text{NH}_4^+$	
	3168 <sup>c</sup>	<b>3I</b>	H <sub>2</sub> O bending overtones or $\text{NH}_4^+$ combination bands	
	3045	<b>3I</b>	asymmetric bonded NH of $\text{NH}_4^+$	
	2962	<b>3I</b>	symmetric bonded NH of $\text{NH}_4^+$	
	$\text{NH}_4^+(\text{H}_2\text{O})_4$	3825	<b>4I–4III</b>	<sup>R</sup> Q <sub>3</sub> , asymmetric free OH of 1° or 2° H <sub>2</sub> O(A)
		3771	<b>4I–4III</b>	<sup>R</sup> Q <sub>1</sub> , asymmetric free OH of 1° or 2° H <sub>2</sub> O(A)
3710 <sup>d</sup>		<b>4I–4III</b>	<sup>P</sup> Q <sub>1</sub> , asymmetric free OH of 1° or 2° H <sub>2</sub> O(A)	
3710 <sup>d</sup>		<b>4II, 4III</b>	free OH of 1° H <sub>2</sub> O(AD)–A or 1° H <sub>2</sub> O(AD)–AA	
3642		<b>4I–4III</b>	symmetric free OH of 1° or 2° H <sub>2</sub> O(A)	
3543		<b>4II</b>	asymmetric bonded OH of 1° H <sub>2</sub> O(AD)–AA	
3408		<b>4III</b>	bonded OH of 1° H <sub>2</sub> O(AD)–A	
3391		<b>4II</b>	free NH of $\text{NH}_4^+$	
3382 <sup>d</sup>		<b>4III</b>	free NH of $\text{NH}_4^+$	
3213 <sup>c</sup>		<b>4I–4III</b>	H <sub>2</sub> O bending overtones or $\text{NH}_4^+$ combination bands	
3116		<b>4I</b>	asymmetric bonded NH of $\text{NH}_4^+$	
3075 <sup>c</sup>		<b>4II, 4III</b>	bonded NH of $\text{NH}_4^+$	
2959 <sup>c</sup>		<b>4II, 4III</b>	bonded NH of $\text{NH}_4^+$	
2779 <sup>c</sup>		<b>4III</b>	bonded NH of $\text{NH}_4^+$	
$\text{NH}_4^+(\text{H}_2\text{O})_5$		3827	<b>5I–5IV</b>	<sup>R</sup> Q <sub>3</sub> , asymmetric free OH of 1° or 2° H <sub>2</sub> O(A)
		3776	<b>5I–5IV</b>	<sup>R</sup> Q <sub>1</sub> , asymmetric free OH of 1° or 2° H <sub>2</sub> O(A)
		3742	<b>5I–5IV</b>	<sup>R</sup> Q <sub>0</sub> , asymmetric free OH of 1° or 2° H <sub>2</sub> O(A)
	3719	<b>5I–5IV</b>	free OH of 1° H <sub>2</sub> O(AD)–A or 1° H <sub>2</sub> O(AD)–AA	
	3714 <sup>d</sup>	<b>5II</b>	asymmetric free OH of 2° H <sub>2</sub> O(AA)	
	3649	<b>5I–5IV</b>	symmetric free OH of 1° or 2° H <sub>2</sub> O(A)	
	3631	<b>5II</b>	symmetric free OH of 2° H <sub>2</sub> O(AA)	
	3562 <sup>d</sup>	<b>5II</b>	asymmetric bonded OH of 1° H <sub>2</sub> O(AD)–AA	
	3551 <sup>d</sup>	<b>5II</b>	symmetric bonded OH of 1° H <sub>2</sub> O(AD)–AA	
	3449	<b>5I</b>	bonded OH of 1° H <sub>2</sub> O(AD)–A	
	3376	<b>5III, 5IV</b>	bonded OH of 1° H <sub>2</sub> O(AD)–AD	
	3217 <sup>c</sup>	<b>5I–5IV</b>	H <sub>2</sub> O bending overtones or $\text{NH}_4^+$ combination bands	
	3133 <sup>c</sup>	<b>5I–5IV</b>	bonded NH of $\text{NH}_4^+$	
	3080 <sup>c</sup>	<b>5II</b>	bonded NH of $\text{NH}_4^+$	
	2892 <sup>c</sup>	<b>5I–5IV</b>	bonded NH of $\text{NH}_4^+$	
$\text{NH}_4^+(\text{H}_2\text{O})_6$	3774	<b>6I–6V</b>	<sup>R</sup> Q <sub>1</sub> , asymmetric free OH of 1°, 2°, or 3° H <sub>2</sub> O(A)	
	3740	<b>6I–6V</b>	<sup>R</sup> Q <sub>0</sub> , asymmetric free OH of 1°, 2°, or 3° H <sub>2</sub> O(A)	
	3719	<b>6I–6V</b>	free OH of 1° H <sub>2</sub> O(AD)–A or 1° H <sub>2</sub> O(AD)–AA	
	3688	<b>6I</b>	free OH of 2° H <sub>2</sub> O(AAD)–A	
	3651	<b>6I–6V</b>	symmetric free OH of 1°, 2°, or 3° H <sub>2</sub> O(A)	
	3567 <sup>d</sup>	<b>6III, 6IV</b>	asymmetric bonded OH of 1° H <sub>2</sub> O(AD)–AA	
	3554 <sup>d</sup>	<b>6III, 6IV</b>	symmetric bonded OH of 1° H <sub>2</sub> O(AD)–AA	
	3494	<b>6I</b>	asymmetric bonded OH of 1° H <sub>2</sub> O(AD)–AAD	
	3463	<b>6I</b>	symmetric bonded OH of 1° H <sub>2</sub> O(AD)–AAD	
	3394	<b>6I</b>	bonded OH of 2° H <sub>2</sub> O(AAD)–A	
	3227 <sup>c</sup>	<b>6I–6V</b>	H <sub>2</sub> O bending overtones or $\text{NH}_4^+$ combination bands	
	3146 <sup>c</sup>	<b>6I–6V</b>	bonded NH of $\text{NH}_4^+$	
	3053 <sup>c</sup>	<b>6I–6V</b>	bonded NH of $\text{NH}_4^+$	
2960 <sup>c</sup>	<b>6I–6V</b>	bonded NH of $\text{NH}_4^+$		

<sup>a</sup> Structures of the isomers are illustrated in Figure 3. <sup>b</sup> The abbreviations used to describe the forms of hydrogen bonding are as follows: single-acceptor (A), double-acceptor (AA), single-acceptor–single-donor (AD), double-acceptor–single-donor (AAD). The dashes denote hydrogen bonding with the perturbing H<sub>2</sub>O in the form of A, AA, AD, or AAD (see text for details). <sup>c</sup> Tentative assignments. <sup>d</sup> Obtained after deconvolution.

isomer **4II** by its characteristic free-NH and bonded-OH absorptions at 3391 and 3543  $\text{cm}^{-1}$ , respectively. For isomer **4III**, which involves a linear water dimer and contains one of each free-NH, free-OH, and bonded-OH stretches, the respective absorptions are located at 3382,  $\sim$ 3710, and 3408  $\text{cm}^{-1}$  [Figure 6b]. The finding that isomer **4III** is preferentially produced in a hotter beam agrees well with the ab initio calculations that this isomer is  $\sim$ 0.7 kcal/mol higher in energy than **4II**.

The presence of structural isomers is not only revealed by the bonded-OH stretches but is also reflected in the bonded-NH stretches where distinct absorptions are recorded. Figure 7 displays the spectra in this region and compares them with the ab-initio-calculated results. Since Figure 6 confirms that isomer **4I** dominates the spectrum, irrespective of the beam temperature, the prominent features at 3116 and 3213  $\text{cm}^{-1}$  in both parts a and b of Figure 7 should be ascribed to the ion

core vibrations of this particular cluster. We notice, however, that isomer **4I** can only exhibit a single absorption for bonded-NH stretches, owing to structural symmetry. If one assigns the most intense feature centered at 3116  $\text{cm}^{-1}$  (fwhm  $\sim$  50  $\text{cm}^{-1}$ ) in Figure 7 to this asymmetric triply degenerate  $\nu_3$  vibration, the higher-frequency feature should, thus, be attributed to H<sub>2</sub>O bending overtones or the combination mode of valence-NH stretching with hydrogen-bond vibrations resonant at  $\sim$ 105  $\text{cm}^{-1}$ . The assignment of the 3213  $\text{cm}^{-1}$  band to the latter is tentative, although it is supported by the ab initio calculations, which predict more than two low-frequency modes resonating at 100–200  $\text{cm}^{-1}$ .<sup>32</sup> Notably, the similar absorption (denoted by an asterisk) is also observed at  $n = 3$ , while its intensity is relatively weaker in comparison.

The temperature dependence measurements in Figure 7 allow for preliminary identification of the bonded-NH stretches of

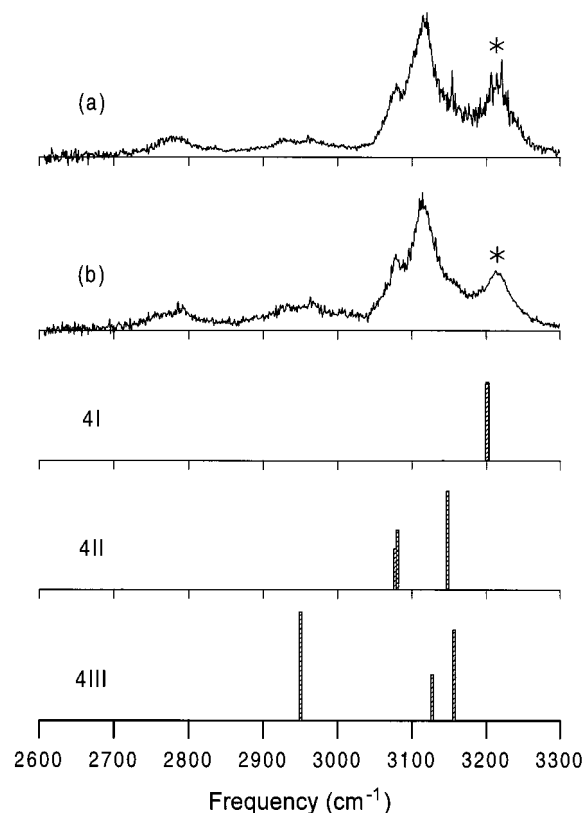


**Figure 7.** Temperature dependence of the vibrational spectra of  $\text{NH}_4^+(\text{H}_2\text{O})_4$  in the NH stretching region. The beam was expanded at a (nozzle temperature, backing pressure) of (a) (250 K, 90 Torr) and (b) (310 K, 60 Torr). All the spectra are laser-power-normalized. Shown underneath are the ab-initio-calculated stick diagrams for the isomers with structures illustrated in Figure 3b. The asterisks denote  $\text{H}_2\text{O}$  bending overtones or  $\text{NH}_4^+$  combination bands.

isomers **4II** and **4III**. Comparing calculations with observations suggests that the low-frequency shoulder at  $3080\text{ cm}^{-1}$  and the weak feature at  $2780\text{ cm}^{-1}$  in Figure 7 belong to isomer **4III**, whereas the  $2930\text{ cm}^{-1}$  band could be that of the ring-shaped isomer **4II**. The assignments, however, are tentative, since these features are relatively weak, broad, and not well resolved. Furthermore, the possible presence of the combination bands may complicate the spectrum in an unclear manner.

**C.  $\text{NH}_4^+(\text{H}_2\text{O})_5$ .** Figure 8a illustrates the OH-stretching spectrum of  $\text{NH}_4^+(\text{H}_2\text{O})_5$  synthesized by a hard supersonic expansion. As in the case of  $n = 4$ , the spectrum is highly sensitive to changes in beam temperature (Figure 9). Standing out in the free-OH stretching region is the peak centering at  $3719\text{ cm}^{-1}$ , which has been identified earlier<sup>35</sup> as the free-OH stretching of two-coordinated  $\text{H}_2\text{O}$ . For bonded-OH stretches, the transitions can be separated into three groups at  $3376$ ,  $3449$ , and  $3559\text{ cm}^{-1}$ . Their absorption intensities vary independently with beam temperature (Figure 9), suggesting that at least three structural isomers are synthesized by the free jet expansion at  $n = 5$ . In Figure 8a, since the  $3559\text{ cm}^{-1}$  band dominates the spectrum in the bonded-OH stretching region, the predominant species should have a structure containing a four-membered ring like isomer **4II**. This is indeed confirmed by the ab initio calculations, which predict that isomer **5II** is one of the lowest-energy structures in Figure 3c. Shown underneath the spectrum in Figure 8a is the calculated stick diagram of isomer **5II**. The close match of the observations with the calculations in both absolute frequencies and relative intensities unambiguously identifies this isomer in the jet.

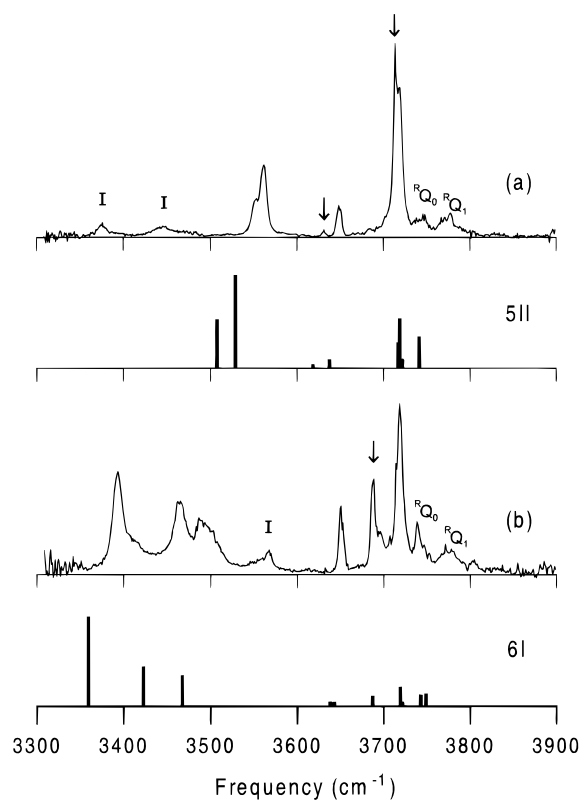


**Figure 8.** Vibrational spectra of cold (a)  $\text{NH}_4^+(\text{H}_2\text{O})_5$  and (b)  $\text{NH}_4^+(\text{H}_2\text{O})_6$  cluster ions in the OH stretching region. The beam was expanded at a nozzle temperature of 250 K and a backing pressure of 200 Torr. Arrows denote (a) the symmetric and asymmetric free-OH stretching absorptions of AA  $2^\circ$   $\text{H}_2\text{O}$  in **5II** and (b) the free-OH stretch of three-coordinated  $\text{H}_2\text{O}$  in **6I**. The bands labeled by “I” are the bonded-OH stretches of (a) isomers **5I**, **5III**, and **5IV** and (b) isomers **6III** and **6IV**. Shown underneath are the ab-initio-calculated stick diagrams of isomers **5II** and **6I** in (a) and (b), respectively.

A number of noticeable characteristics support the identification of isomer **5II** in Figure 8a. First, the calculations predict a splitting of  $21\text{ cm}^{-1}$  for the two-coupled bonded-OH stretches involved in the four-membered ring. This can be compared to the observed splitting of  $11\text{ cm}^{-1}$ , obtained after deconvolution of the  $3559\text{ cm}^{-1}$  band with two Gaussian profiles. Second, the calculated relative intensity of the asymmetric ( $3528\text{ cm}^{-1}$ ) to the symmetric ( $3507\text{ cm}^{-1}$ ) absorption is about 2:1 (Table 4), which agrees nearly excellently with the observation. Third, the double-acceptor (AA)  $\text{H}_2\text{O}$  that comprises the symmetric ring can be identified by the spectrum. The  $\text{H}_2\text{O}(\text{AA})$  differs from  $\text{H}_2\text{O}(\text{A})$  in two ways: (1) it cannot freely locally rotate and (2) its stretching frequencies red-shift more because of double hydrogen bonding. These two distinct features can be found as the weak absorptions at  $3631$  and  $3714\text{ cm}^{-1}$ , ascribed to the symmetric and asymmetric stretching vibrations of this  $2^\circ$   $\text{H}_2\text{O}(\text{AA})$ , respectively. While the  $3714\text{ cm}^{-1}$  band is severely overlapped with the free-OH stretching of  $1^\circ$   $\text{H}_2\text{O}(\text{AD})$  at  $3719\text{ cm}^{-1}$ , it can be well isolated after deconvolution.

Figure 3c also illustrates the ab-initio-optimized geometries of other low-energy isomers of  $\text{NH}_4^+(\text{H}_2\text{O})_5$ . The isomers, except **5IV**, share one trait in common: the first hydration shell is entirely filled with no free-NH bonds exposed. As noted from Table 2, the symmetric ring structure (**5II**) is lowest in energy.<sup>32</sup> This calculation correlates well with the observation that isomer **5II** is preferentially formed upon lowering the beam temperature. Figure 9 compares the calculated stick spectra with that obtained at a higher beam temperature. The assignment

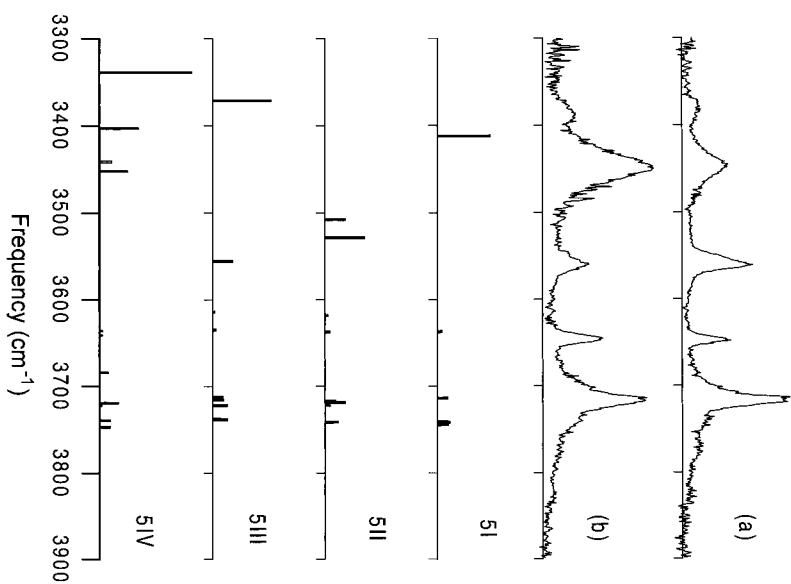


**Figure 9.** Temperature dependence of the vibrational spectra of  $\text{NH}_4^+(\text{H}_2\text{O})_5$  in the OH stretching region. The beam was expanded at a nozzle temperature, backing pressure) of (a) (280 K, 80 Torr) and (b) (300 K, 60 Torr). All the spectra are laser-power-normalized. Shown underneath are the ab-initio-calculated stick diagrams of NH ( $\square$ ) and OH ( $\bullet$ ) for the isomers with structures illustrated in Figure 3c.

of the bonded-OH stretching absorptions at 3448  $\text{cm}^{-1}$  to **5I** is clear but is less unambiguous for the 3383  $\text{cm}^{-1}$  band, which can either belong to isomer **5III** or **5IV**. Initially, it appears that the absorption should be attributed to isomer **5IV**, which is 2–3 kcal/mol more stable. However, the assignment is inconclusive since this isomer, containing a three-coordinated  $\text{H}_2\text{O}$ , should display a characteristic free-OH stretching absorption at  $\sim 3690 \text{ cm}^{-1}$ .<sup>35</sup> This evidence remains missing in the spectrum.

In the NH stretching region, the  $\text{NH}_4^+(\text{H}_2\text{O})_5$  spectrum (Figure 10) is rather complex. The observation is analogous to that of  $\text{NH}_4^+(\text{NH}_3)_5$  (ref 15) where the  $T_d$  symmetry of the ammonium ion core is broken. An additional factor complicating the spectrum is the presence of more than three structural isomers whose bonded-NH stretching absorptions substantially overlap each other. The breadths of the features observed in Figure 10 are typically more than 50  $\text{cm}^{-1}$ , preventing a precise determination of their identities and, ultimately, their spectral assignments. The only obvious difference found in the temperature-dependent measurement in Figure 10 is the emergence of the new band at 3080  $\text{cm}^{-1}$  as the beam is cooled. In accord with the conclusion drawn from the OH spectra, this band should be ascribed to the ion-core stretching of **5II**, and the prominent feature at 3133  $\text{cm}^{-1}$  is primarily due to isomer **5I**. The water bending overtones and/or the ion-core combination bands are also observed at 3217  $\text{cm}^{-1}$ .

**D.  $\text{NH}_4^+(\text{H}_2\text{O})_6$ .** Figure 8 compares the low-temperature spectra of  $\text{NH}_4^+(\text{H}_2\text{O})_6$  and  $\text{NH}_4^+(\text{H}_2\text{O})_5$  in the OH stretching region. Notably, as  $n$  increases, the intensity of the ring mode at 3559  $\text{cm}^{-1}$  markedly decreases. This event is accompanied by the appearance of the new features at 3394, 3463, and 3494

**Table 4.** Ab-Initio-Calculated NH and OH Stretching Frequencies ( $\text{cm}^{-1}$ ) and Absorption Intensities ( $\text{km/mol}$ ) of  $\text{NH}_4^+(\text{H}_2\text{O})_{3-6}$ , using B3LYP/6-31+G<sup>\*a</sup>

frequency (intensity)												
isomer <b>3I</b>	isomer <b>4I</b>	isomer <b>4II</b>	isomer <b>4III</b>	isomer <b>5I</b>	isomer <b>5II</b>	isomer <b>5III</b>	isomer <b>5IV</b>	isomer <b>6I</b>	isomer <b>6II</b>	isomer <b>6III</b>	isomer <b>6IV</b>	isomer <b>6V</b>
3735 (133)	3739 (154)	3737 (133)	3741 (120)	3744 (117)	3741 (83)	3738 (168)	3747 (130)	3748 (127)	3741 (134)	3749 (114)	3725 (83)	3743 (116)
3734 (129)	3739 (145)	3720 (39)	3739 (134)	3741 (136)	3741 (158)	3737 (77)	3739 (128)	3743 (114)	3741 (121)	3745 (114)	3724 (5)	3742 (117)
3734 (143)	3739 (165)	3717 (274)	3737 (123)	3741 (110)	3722 (41)	3722 (164)	3722 (22)	3742 (118)	3740 (103)	3724 (44)	3721 (263)	3718 (71)
3634 (16)	3738 (27)	3713 (133)	3711 (115)	3741 (105)	3718 (254)	3715 (113)	3719 (234)	3721 (26)	3716 (108)	3721 (256)	3721 (264)	3716 (119)
3634 (42)	3636 (1)	3636 (32)	3637 (28)	3714 (108)	3717 (127)	3712 (122)	3684 (104)	3719 (212)	3713 (131)	3719 (125)	3718 (114)	3713 (211)
3634 (49)	3636 (40)	3615 (15)	3636 (22)	3637 (19)	3637 (16)	3635 (23)	3641 (28)	3687 (104)	3688 (98)	3714 (100)	3718 (114)	3711 (106)
3429 (101)	3636 (38)	3519 (527)	3635 (39)	3637 (10)	3637 (38)	3634 (37)	3636 (31)	3642 (26)	3637 (26)	3641 (21)	3618 (7)	3638 (17)
3116 (1157)	3636 (40)	3496 (265)	3434 (90)	3637 (40)	3618 (14)	3614 (21)	3452 (350)	3638 (23)	3636 (24)	3639 (25)	3618 (18)	3637 (34)
3116 (1158)	3201 (906)	3438 (110)	3381 (753)	3637 (37)	3528 (483)	3555 (251)	3441 (155)	3637 (29)	3635 (34)	3619 (13)	3534 (0)	3616 (16)
3084 (172)	3201 (886)	3148 (1137)	3156 (1031)	3412 (666)	3507 (250)	3371 (744)	3403 (493)	3467 (358)	3489 (369)	3535 (463)	3532 (944)	3536 (311)
	3200 (885)	3080 (688)	3127 (521)	3227 (804)	3228 (822)	3288 (390)	3339 (1157)	3422 (467)	3348 (523)	3515 (243)	3513 (244)	3502 (473)
	3141 (0)	3077 (473)	2950 (1238)	3225 (809)	3213 (1064)	3208 (913)	3165 (1051)	3359 (1088)	3332 (1027)	3430 (624)	3513 (244)	3365 (772)
				3179 (441)	3170 (529)	3165 (378)	3052 (697)	3243 (781)	3231 (744)	3242 (898)	3226 (1415)	3245 (770)
				3064 (844)	3141 (113)	2949 (986)	3045 (661)	3217 (983)	3221 (972)	3206 (460)	3207 (477)	3220 (874)
								3136 (502)	3170 (165)	3183 (683)	3207 (477)	3161 (322)
								3121 (358)	2978 (879)	3091 (700)	3154 (0)	3015 (909)

<sup>a</sup> Structures of the isomers are illustrated in Figure 3. The frequencies underlined are those of (1) bonded-OH stretches involving an unperturbed symmetric four-membered ring in isomers **4II**, **5II**, **6III**, and **6IV** and (2) free-OH stretches of three-coordinated  $\text{H}_2\text{O}$  in isomers **5IV**, **6I**, and **6II**. The frequencies are all scaled by a factor of 0.973.

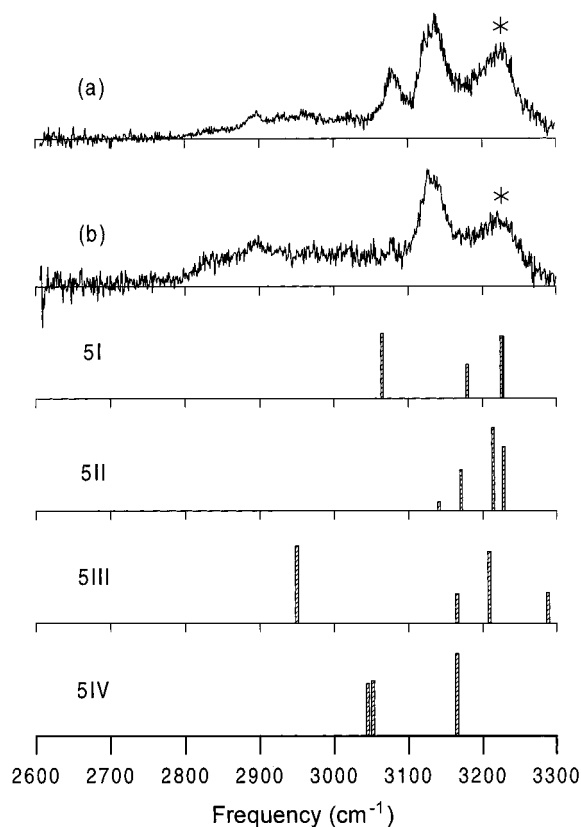


**Figure 10.** Temperature dependence of the vibrational spectra of  $\text{NH}_4^+(\text{H}_2\text{O})_5$  in the NH stretching region. The beam was expanded at a (nozzle temperature, backing pressure) of (a) (250 K, 110 Torr) and (b) (300 K, 60 Torr). All the spectra are laser-power-normalized. Shown underneath are the ab-initio-calculated stick diagrams for the isomers with structures illustrated in Figure 3c. The asterisks denote  $\text{H}_2\text{O}$  bending overtones or  $\text{NH}_4^+$  combination bands.

$\text{cm}^{-1}$  for the bonded-OH stretches. The free-OH stretching, however, retains its resonance nearly at the same frequency ( $3719 \text{ cm}^{-1}$ ) along with a new band emerging at  $3688 \text{ cm}^{-1}$  for three-coordinated  $\text{H}_2\text{O}$ .<sup>35</sup> The two free-OH stretching features are well resolved with a fwhm of  $\sim 8 \text{ cm}^{-1}$  for each absorption. Figure 3d depicts five low-energy structures of  $\text{NH}_4^+(\text{H}_2\text{O})_6$ , of which the one (**6I**) having a three-coordinated  $\text{H}_2\text{O}$  is lowest in energy. Among these five isomers, the species **6I** is expected to dominate the observed spectrum not only because it is energetically more stable but also because it can be synthesized most easily from isomer **5II**. This is indeed confirmed by comparing the low-temperature spectrum with the ab-initio-calculated stick diagram in Figure 8b. Remarkably, the observed features that can be ascribed to the two distinct free-OH and three bonded-OH stretching vibrations of isomer **6I** match nearly perfectly with those predicted. Although isomer **6II** also contains a three-coordinated  $\text{H}_2\text{O}$ , it is less stable by more than 2 kcal/mol.

Similar to  $\text{NH}_4^+(\text{H}_2\text{O})_{4,5}$ ,  $\text{NH}_4^+(\text{H}_2\text{O})_6$  has a spectrum that is sensitive to beam temperature changes as well. This is seen when comparing Figure 8b with Figure 11 where the spectrum was obtained at a higher beam temperature. In Figure 11, we also show the ab-initio-calculated diagrams of isomeric  $\text{NH}_4^+(\text{H}_2\text{O})_6$  in both NH and OH stretching regions for comparison. The calculated relative stability of these isomers using B3LYP/6-31+G\* is given in Table 2. Resembling that of  $\text{NH}_4^+(\text{H}_2\text{O})_5$ , the observed NH stretching transitions are too complicated to be unambiguously assigned because of interference from isomers and also blending of the fundamental transitions with the

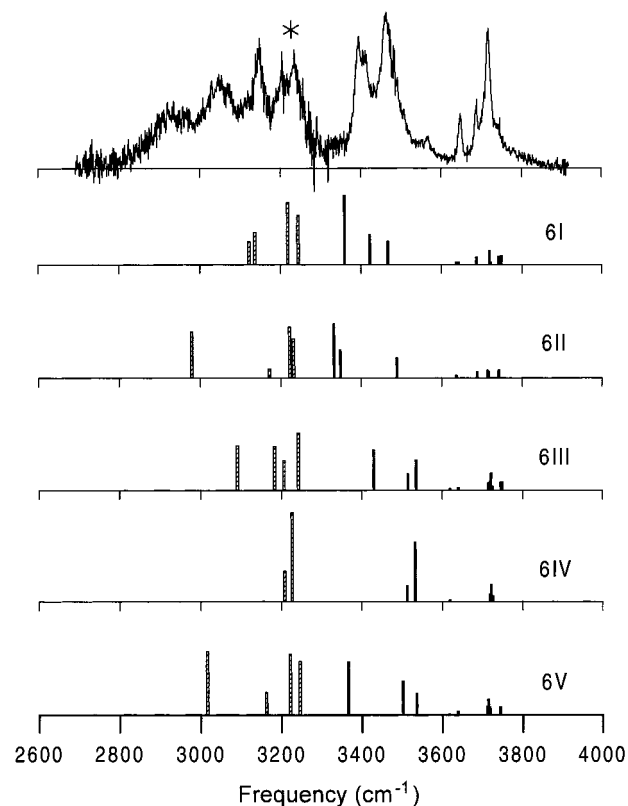


**Figure 11.** Vibrational spectrum of  $\text{NH}_4^+(\text{H}_2\text{O})_6$  in both the NH and OH stretching regions. The beam was expanded at a nozzle temperature of 310 K and a backing pressure of 90 Torr. Shown underneath are the ab-initio-calculated stick diagrams of NH ( $\square$ ) and OH ( $\blacksquare$ ) stretches for the isomers with structures illustrated in Figure 3d. The asterisk denotes  $\text{H}_2\text{O}$  bending overtones or  $\text{NH}_4^+$  combination bands.

combination bands. For OH stretches, unambiguous identification can be made only for the absorptions at  $\sim 3690$  and  $\sim 3550 \text{ cm}^{-1}$  arising, respectively, from the free-OH stretching of three-coordinated  $\text{H}_2\text{O}$  and the bonded-OH stretches of  $1^\circ \text{H}_2\text{O}(\text{AD})$  perturbed by  $2^\circ \text{H}_2\text{O}(\text{AA})$ .

Benefiting from the jet cooling effect, the absorptions near  $3550 \text{ cm}^{-1}$  can be fully uncovered in the lower-temperature spectrum of Figure 8b. The band, originally observed for **5II**, is asymmetric with a central frequency ( $3567 \text{ cm}^{-1}$ ) agreeing with that of the ring-shaped  $\text{NH}_4^+(\text{H}_2\text{O})_5$  to within  $10 \text{ cm}^{-1}$ . Furthermore, it is shaded to the red, a characteristic of two-coupled, equivalent oscillators. Since this band is the fingerprint of an unperturbed symmetric four-membered ring, its observation suggests that both the isomers **6III** and **6IV** could be produced along with **6I** by the free jet expansion. The suggestion is fully corroborated by the ab initio calculations for these two isomers whose stick spectra are presented in Figure 11. Since isomer **6IV** is  $\sim 0.7 \text{ kcal/mol}$  more stable than **6III**, as predicted by the calculations, the  $3567 \text{ cm}^{-1}$  band observed in Figure 8b should predominantly originate from **6IV**, that is, a symmetric double-ring species.

The intriguing “figure-eight-shaped” double-ring isomer has a highly simplified spectrum in both the OH and NH stretching regions. The species is linked together by eight hydrogen bonds, forming a robust structure somewhat similar to that of the cagelike  $(\text{H}_2\text{O})_6$ .<sup>7</sup> The stress enforced on the  $\text{NH}_4^+$  central ion by the hydrogen bonds is relatively large, resulting in a tightening of the two interconnected NH bonds by about  $3^\circ$ . Furthermore, upon ring closure, the directionality of all the hydrogen bonds is substantially reduced to  $\angle \text{N}-\text{H}\cdots\text{O} = 160.0^\circ$  and  $\angle \text{O}-\text{H}\cdots\text{O} = 162.7^\circ$ . With the four free-OH bonds of

the  $1^\circ$   $\text{H}_2\text{O}(\text{AD})$  molecules lying separately in two perpendicular ring planes, a symmetry of  $D_{2d}$  is achieved. This unique structure is inherited naturally from the tetrahedral geometry of the ammonium central ion.

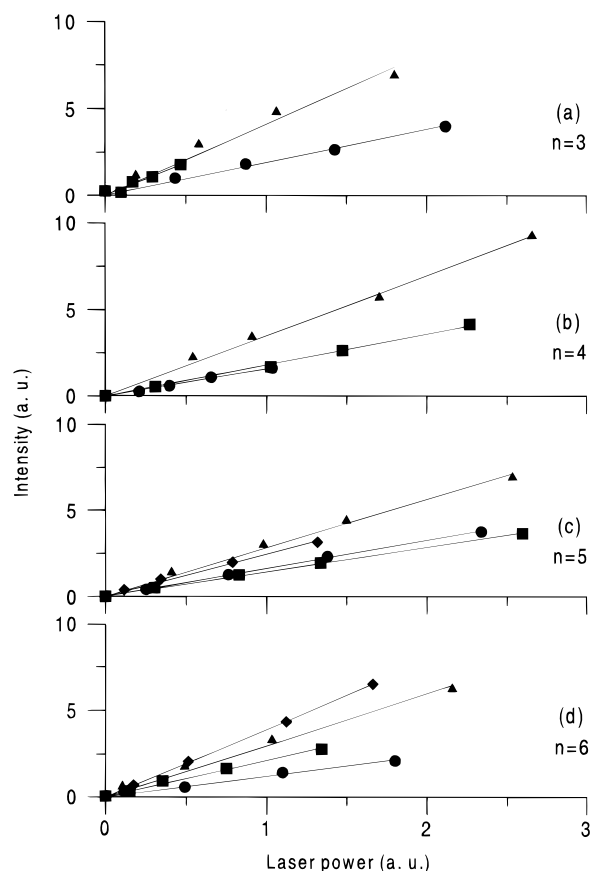
Finally, it is worth noting that the species containing a five-membered ring<sup>43</sup> can also be one of the low-energy isomers of  $\text{NH}_4^+(\text{H}_2\text{O})_6$ . The five-membered ring structure **6V**, analogous to **5II**, has an energy higher than **6III** by  $\sim 0.6$  kcal/mol. It is highly likely that this isomer was produced in the hotter beam as well (Figure 11); however, lacking a three-coordinated  $\text{H}_2\text{O}$ , it should contribute insignificantly to the spectrum displayed in Figure 8b where an intense absorption is observed at  $3688\text{ cm}^{-1}$ . Additional evidence ruling out the presence of isomer **6V** in the colder beam lies in its computed frequencies and intensities for the bonded-OH stretches. These values (Table 4 and Figure 11) poorly match with the observations [Figure 8b] of both absolute frequencies and relative intensities of the ring vibrations.

### Discussion

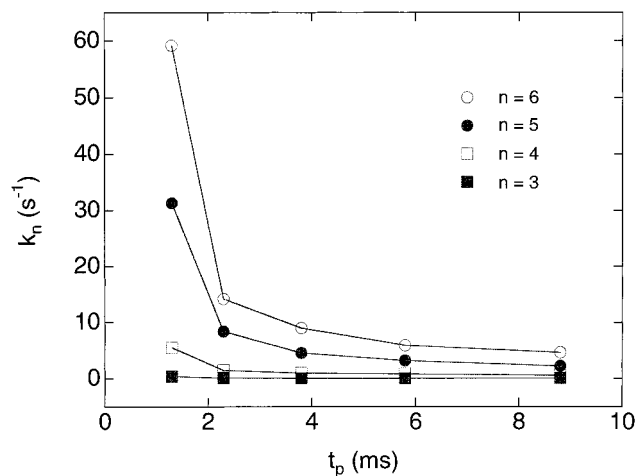
Substantiated by the temperature dependence measurements, the present spectroscopic investigations of  $\text{NH}_4^+(\text{H}_2\text{O})_n$  have successfully identified a number of structural isomers. To further characterize these cluster ions, we determined the power dependence of the spectra and the internal energies accommodated by the isomers. Such a determination would not only provide useful energetics information but also reveal the details of how fragmentation occurs upon laser excitation. The knowledge is crucial for quantitatively understanding the nature of the photofragmentation processes.

Figure 12 displays the dependence on laser pulse energy of the fragment signals from photofragmentation of  $\text{NH}_4^+(\text{H}_2\text{O})_{3-6}$ . All vibrational modes of the clusters behave similarly, with the detected signals depending linearly on laser energy. The linear dependence indicates that the vibrationally induced dissociation upon stretching excitation is a single-photon process. This result is surprising, since an infrared photon of  $3000\text{ cm}^{-1}$  contains only  $8.6$  kcal/mol, which is lower than the incremental hydration energies determined by thermochemistry in Table 1. We note that a similar linear power dependence has been previously reported for  $\text{NO}^+(\text{H}_2\text{O})_{2,3}$ . Choi et al.<sup>44</sup> contended that the one-photon dissociation can occur because a substantial amount of internal energy is accessible in the cluster ions generated by electron bombardment. The critical role the internal energy plays is also emphasized in the study of  $\text{NH}_4^+(\text{NH}_3)_{6-9}$ . When vibrationally exciting the cluster ions using a CW  $\text{CO}_2$  laser at  $10\text{ }\mu\text{m}$ , Ichihashi et al.<sup>16</sup> successfully obtained the  $\nu_2$  vibration spectra of the solvent  $\text{NH}_3$  molecules. Although the energy supplied by each  $\text{CO}_2$  laser photon is only  $3.0$  kcal/mol, which is insufficient to overcome the dissociation barrier of  $\sim 7$  kcal/mol, the excessive amount of internal energy in the vibrationally hot ions can compensate for the energy deficit.

Also well documented, the CW corona-discharge-generated metastable species after free jet expansion remain vibrationally hot. For small radicals such as  $\text{OH}$ ,<sup>45</sup> the vibrational temperature can rise up to  $3400\text{ K}$ , accompanied by a low rotational temperature of  $11\text{ K}$ . For larger clusters, the vibrational temperature can be substantially lowered because of internal cooling via energy redistribution to intermolecular low-



**Figure 12.** Power dependence of the individual vibrational transitions of  $\text{NH}_4^+(\text{H}_2\text{O})_{3-6}$  at wavenumbers of (a) 3378 (■), 3641 (▲), 3717 (●); (b) 3415 (●), 3646 (▲), 3729 (■); (c) 3449 (◆), 3558 (■), 3647 (●), 3717 (▲); (d) 3150 (◆), 3393 (■), 3651 (●), 3718 (▲).



**Figure 13.** Changes of the evaporation rate constants ( $k_n$ ) of  $\text{NH}_4^+(\text{H}_2\text{O})_{3-6}$  as a function of trapping time ( $t_p$ ).

frequency modes, or the heat sink. The cooling can be further facilitated by evaporation where the desorbing molecules carry away parts of the internal energies. In line with previous studies,<sup>16</sup> we estimated the internal temperature of the clusters by measuring the unimolecular dissociation rate constant ( $k_n$ ) of the evaporation,



Figure 13 displays the typical rate constants obtained as a function of trapping time ( $t_p$ ) for various clusters. As expected,

(43) The intriguing five-membered ring structure has been clearly identified for protonated methanol pentamers [Chang, H.-C.; Jiang, J. C.; Lin, S. H.; Lee, Y. T.; Chang, H.-C. *J. Am. Chem. Soc.*, submitted].

(44) Choi, J.-H.; Kuwata, K. T.; Haas, B.-M.; Cao, Y.; Johnson, M. S.; Okumura, M. *J. Chem. Phys.* **1994**, *100*, 7153.

(45) Droege, A. T.; Englekling, P. C. *Chem. Phys. Lett.* **1983**, *96*, 316.

the  $k_n$  decays nearly exponentially with  $t_p$ , an evidence of evaporative cooling of the trapped ions. The larger clusters dissociate more rapidly (with a larger  $k_n$ ) because of weaker hydrogen bonding between the dissociating H<sub>2</sub>O and the ammonium ion core. Applying the evaporating ensemble theory of Klots<sup>46</sup> to the present system indicates that the clusters interrogated in this experiment have an internal temperature ranging from ~130 to ~170 K at  $n = 6$  to  $n = 3$ . The temperatures are comparable to those estimated for protonated water clusters H<sup>+</sup>(H<sub>2</sub>O)<sub>5–65</sub> produced by corona discharge and cooled in an electromagnetic ion trap under collision-free conditions.<sup>47</sup>

With these internal temperatures, we calculated explicitly the internal energies of the clusters based on harmonic-oscillator approximations and the frequencies of all vibrational modes provided by the ab initio calculations. Given at the temperatures of 130–170 K, the clusters accommodate most of their internal energies in the intermolecular vibrational modes, which all resonate at the frequency lower than 800 cm<sup>-1</sup>. Rough estimation indicates that the internal energies of isomers **3I**, **4I**, **5II**, and **6I** at 150 K are 2.0, 3.0, 3.1, and 4.0 kcal/mol, respectively. The difference in energy between isomers of the same solvation group is less than 1 kcal/mol. Notably, the content of these internal energies is sufficient to compensate for a large portion of the energy deficit between the absorbed infrared photon and the dissociation barrier. It means that most of the species can dissociate upon one-photon excitation, and the dissociation is not limited to the species located at the high-energy tails of the Boltzmann distribution.

This experiment involves using a pulsed infrared laser to obtain the spectra. Two-photon excitation may also occur as the clusters are exposed to the infrared radiation with a peak power density on the order of 10<sup>7</sup> W/cm<sup>2</sup>. Absorbing two photons places the clusters in the excited states embedded in a quasi-continuum where the clusters can rapidly predissociate. However, according to the present observations (Figure 12), we exclude this possibility and conclude that the absorption cross section of the second photon is small such that no significant traces of quadratic power dependence can be detected for NH<sub>4</sub><sup>+</sup>(H<sub>2</sub>O)<sub>3–6</sub>. This conclusion is unsurprising since the second photon involves an off-resonant excitation, although the density of states is much higher at the first overtone region. The evidence of single-photon excitation suggests that the photo-fragmentation observed in the present study should be better understood as a convoluted process of vibrational predissociation with photoevaporation.<sup>48</sup>

The power dependence measurements, unfortunately, indicate that the presently recorded spectra were derived considerably from internally hot species. Although the species have been stored in the radio frequency ion trap for about 1 ms before inspection, the cooling still cannot eliminate most of the metastable ions. As a result of the insufficient cooling, the observed absorptions are actually the overlapping sequence bands initiating from thermally excited intermolecular low-frequency modes, which can be easily populated at temperatures near 150 K. The transitions recorded in Figures 4–11 are, thus, most likely broadened due to heterogeneous processes. While the observed band intensities are those of vibrationally hot species, the linear power dependence demonstrates that semi-quantitative estimates concerning the relative absorption strengths

of the valence bond vibrations and the relative abundance of isomers in the jet can be obtained from the spectra.

Also revealed by the temperature dependence measurements are the clustering kinetics of NH<sub>4</sub><sup>+</sup>(H<sub>2</sub>O)<sub>*n*</sub> upon the supersonic expansion. As an interesting contrast, the effect of cooling on varying the vibrational predissociation spectrum is relatively small at  $n = 4$  but is dramatic at  $n = 5$ . This effect is particularly manifested for ring isomers whose temperature-dependent behaviors markedly differ between these two cases. The intriguing difference could be properly accounted for by considering kinetic effects, in addition to energetics. We assume that, during the process of ring formation, the linear isomers **4III** and **5I** must be first synthesized. The rate of their synthesis subsequently determines the final observation of the ring-shaped species. For NH<sub>4</sub><sup>+</sup>(H<sub>2</sub>O)<sub>4</sub>, the spectrum in Figure 6b reveals that most of the clusters are already populated at the **4I** potential well when the beam is warm. Attempts to increase the concentration of the intermediate **4III** by cooling are energetically unfavorable because the species is ~2 kcal/mol less stable than **4I**. Observing **4II** is thus inhibited by the inefficiency of forming the intermediates for ring closure and also by the fact that most of the clusters are trapped at the **4I** noncyclic configuration. This kinetic consideration can be similarly applied to account for the dramatic temperature dependence of the spectra of NH<sub>4</sub><sup>+</sup>(H<sub>2</sub>O)<sub>5</sub>. Since the potential well of the linear isomer **5I** is most probably populated under mild expansion conditions, sufficient cooling can effectively close the ring, yielding the desired structure **5II** as demonstrated in Figures 8a and 9. The same clustering kinetic argument also explains why the growth of isomer **5IV** is limited in the free jet expansion.

## Conclusion

The NH<sub>4</sub><sup>+</sup>(H<sub>2</sub>O)<sub>*n*</sub> cluster ions display a number of interesting spectral features in both NH and OH stretching vibrations. In this work, we have unambiguously identified several structural isomers of NH<sub>4</sub><sup>+</sup>(H<sub>2</sub>O)<sub>3–6</sub> based upon their characteristic stretching transitions and their matches in frequencies and intensities with ab initio calculations. In particular, the ring-shaped isomers are identified, for the first time, for any hydrogen-bonded ionic clusters. The success of this experiment suggests that the VPIT spectrometer is quite appropriate for investigating protonated ion hydration in the gas phase.<sup>37</sup> The intriguing hydrogen bond rearrangement dynamics, as that theoretically examined for neutral water clusters,<sup>49</sup> can be further studied using this apparatus. Together with the thermodynamics data obtained by mass spectrometry and the geometrical configurations predicted by ab initio calculations, the infrared spectroscopic measurements of NH<sub>4</sub><sup>+</sup>(H<sub>2</sub>O)<sub>*n*</sub> provide additional insight not only into the interaction potentials of the ions with the solvent molecules but also into the interactions between the solvent molecules. Such measurements correlate well with the studies of heterogeneous water nucleation, a critical process associated with cloud formation in the atmosphere.<sup>50</sup>

**Acknowledgment.** The authors thank the Academia Sinica and the National Science Council of Taiwan, Republic of China, for financially supporting this research under Contract Nos. NSC 86-2113-M-001-034 and 87-2113-M-001-027-CT.

JA9802908

(46) Klots, C. E. *Z. Phys. D: At., Mol. Clusters* **1991**, *20*, 105.

(47) Schindler, T.; Berg, C.; Niedner-Schatteburg, G.; Bondybey, V. E. *Chem. Phys. Lett.* **1996**, *240*, 301.

(48) Anex, D. S.; Davidson, E. R.; Douketis, C.; Ewing, G. E. *J. Phys. Chem.* **1988**, *92*, 2913.

(49) Wales, D. J.; Ohmine, I. *J. Chem. Phys.* **1993**, *98*, 7257.

(50) Wayne, R. P. *Chemistry of Atmospheres*; Oxford University Press: Oxford, 1991.